ORIGINALS

Wee King Soh · Boo Cheong Khoo · W. Y. Daniel Yuen

The entrainment of air by water jet impinging on a free surface

Abstract High-speed cine and video photographs were used to capture the flow patterns of a column of water jet impinging into a pool of water. The impact results in air entrainment into water in the form of a void with no mixing between the water in the jet and the surrounding water. Conservation of fluid momentum shows that the rate of increase of the height of the air void depends on the drag coefficient of the jet front. By neglecting the frictional losses, the application of energy conservation yields an expression that relates the maximum height of the air void with the properties of the water jet.

1 Introduction

The entrainment of air into a pool of water as a result of water jet impingement has been of interest in many facets of engineering. For a water jet which is continuously pouring into an otherwise calm free surface, the entrainment of air is in the form of bubbles being "dragged" below the free surface. This mechanism has been well studied with recent research in this area represented by the works of Cummings and Chanson (1997) and Bonetto et al. (1994). The analysis of Cummings and Chanson is based on a diffusion process in which the

W. K. Soh (✉)
School of Mechanical, Materials & Mechatronics Engineering,
University of Wollongong, Northfields Ave, 2522, NSW, Australia
E-mail: wksoh@uow.edu.au
Tel.: +61 2 42 213059
Fax: +61 2 42 213238

B. C. Khoo
Department of Mechanical and Production Engineering,
National University of Singapore, 10 Kent Ridge Crescent,
119260, Singapore

W. Y. D. Yuen
BlueScope Steel Research, PO Box 202,
Port Kembla, 2505, NSW, Australia

amount of air entrainment is calculated in terms of an air–water ratio from a diffusion equation. Bonetto et al. (1994) considered the Helmholtz instability on the free surface of the jet as a mechanism for trapping air bubbles into water.

Air entrainment also occurs during a very short time immediately after the water jet makes contact with the horizontal free surface. The collision between the two free surfaces creates free surface waves and resulting air being trapped in a void below the free surface—the phenomenon is dependent on the Froude and Weber numbers.

In an experimental study on the falling of a short water column into water, Oguz et al. (1995) showed features of air entrainment as the column entered the free surface. The study was carried further by Zhu et al. (2000). Their carefully designed flow system produces a column of water that flowed steadily into a pool of water without any disturbance on the free surface. The diameter of the water jet was then perturbed in the nozzle and as the perturbation in the jet reached the horizontal free surface air was entrained into the free surface in the form of a void. The entrainment of air in this form was first observed by Benjamin and Ellis in 1966. In flow visualization of the collapse of a vapor bubble, Benjamin and Ellis discovered penetration of the free surface by a high-speed water micro-jet. The fact that the jet of water was visible in the surrounding water, as shown in the high-speed photograph, is due to a layer of the entrained vapor which separated the impinging jet from the surrounding water. Significant research interest was focused on computer studies of the pulsations of a vapor bubble with the aim to gain further understanding of the mechanism that causes cavitations. In the collapse of a vapor (or gas) bubble in water in the presence of a rigid wall, the side of the bubble away from the wall will concave inward thus forming a thin water jet (micro-jet) penetrating the cavity. In acute situations, the micro-jet will pass through the cavity and strike at the interface on the other side of the cavity. Thus the situation of a water jet impinging on a free surface has occurred. The phe-

nomenon of the impact was first modeled by Best (1993) in which a mathematical cut in the velocity potential was used to represent the continuation of the collided interfaces. Note that the model by Best assumed a velocity of the interface immediately after the impact between the jet and the free surface. Zhang et al. (1993), in their calculations, made use of a vortex sheet to represent the collided interfaces. The trajectories of points on the vortex sheet was traced by the flow-induced velocity vectors that are normal to the vortex sheet. The cohesion of two free surfaces in forming a vortex sheet was an over-simplified model as it did not conserve the momentum of the colliding fluids. It has become necessary to conduct a visualization study of a water jet impacting on a free surface, which may provide the much needed information for the formulation of an impact boundary condition for computer simulation of the impact between a free jet and free surface.

This work came about from the discussion amongst the authors on jet impact problems that are common in industry. Some examples include the welding process where a jet of liquid metal strikes the weld pool, the penetration of a micro-jet during the collapse of a vapor bubble in liquid, and in spray cooling where a cooling jet has to strike at a layer of water floating on a hot surface. The disturbance created by the jet impact and the penetration of the jet will be of interest to the mixing of the two liquids and the characteristics of heat transfer, for example, in the processes of welding and jet cooling.

2 The experiments

A visualization study reported here is similar to the experiments by Oguz et al. (1995). The aim is to observe a long stream of water jet from the moment it makes contact with the free surface.

The apparatus consists of a water feeder tank located above a receiver tank which contains water at a prescribed depth. The height of the feeder tank is adjustable and a nozzle is attached to its bottom through a valve. The receiver tank is transparent so that the interior of the tank is visible. A sudden opening of the valve will release a column of water jet flowing down towards the receiver tank. The velocity of the water jet reaching the free surface in the receiver tank is dependent on the height of the water level at the feeder tank and in the pipe and the control valve. A schematic diagram of the experimental set-up is shown in Fig. 1.

In the experiments, a column of water was released from the feeder tank. As the water jet entered the free surface of the reservoir tank, a high-speed video camera recorded the flow at a rate of 1,000 frames per second and in the case of using a cine camera, the filming rate was 2,000 frames per second. Backlighting was used during the filming with the cine camera in order to have adequate exposure at the required filming rate. The water from the feeder tank was dyed blue so that the
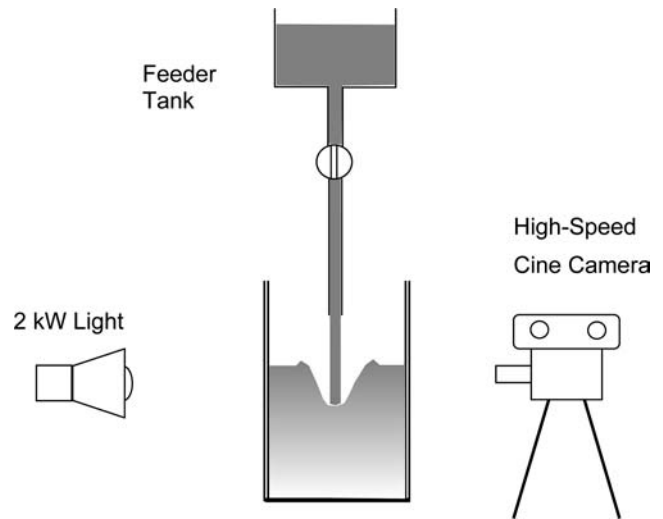

Fig. 1 Schematic diagram of the experimental set-up

movement of the water from the jet inside the receiver tank could be traced.

Relevant experimental data for jets impinging on deep water are shown in Table 1.

3 Observations

A visualization study similar to that of Pumphrey and Elmon (1990) was recorded from a sequence of four water droplets striking the free surface. As shown in Fig. 2, the impact by the first three droplets created a cascade of three hemi-spherical voids. The voids retracted at the time when the fourth droplet impacted the free surface, resulting in a bubble separating from the void and carried downward by the momentum of the droplet. It is evident that steady state virtually existed at

Table 1 A tabulation of experimental data for jet impingement into deep water

Test no.	V_j (m/s)	V_2 (m/s)	Fr	λ
1	0.38	0.30	2.6	0.787
2	0.39	0.21	2.8	0.538
3	0.42	0.26	3.3	0.605
4	0.45	0.39	3.5	0.872
5	0.88	0.63	13.3	0.714
6	1.22	0.76	20.1	0.627
7	1.14	0.79	20.2	0.695
8	1.42	0.91	27.2	0.642
9	1.35	0.78	28.4	0.581
10	1.52	1.00	31.3	0.659
11	1.47	0.90	34.1	0.611
12	1.90	1.12	48.9	0.591
13	1.89	1.03	55.7	0.544
14	2.04	0.90	65.1	0.443
15	2.06	1.12	66.6	0.543

V_j velocity of the jet prior to impingement; V_2 velocity after impingement; Fr Froude number; and $\lambda = V_2/V_j$ is the velocity ratio.
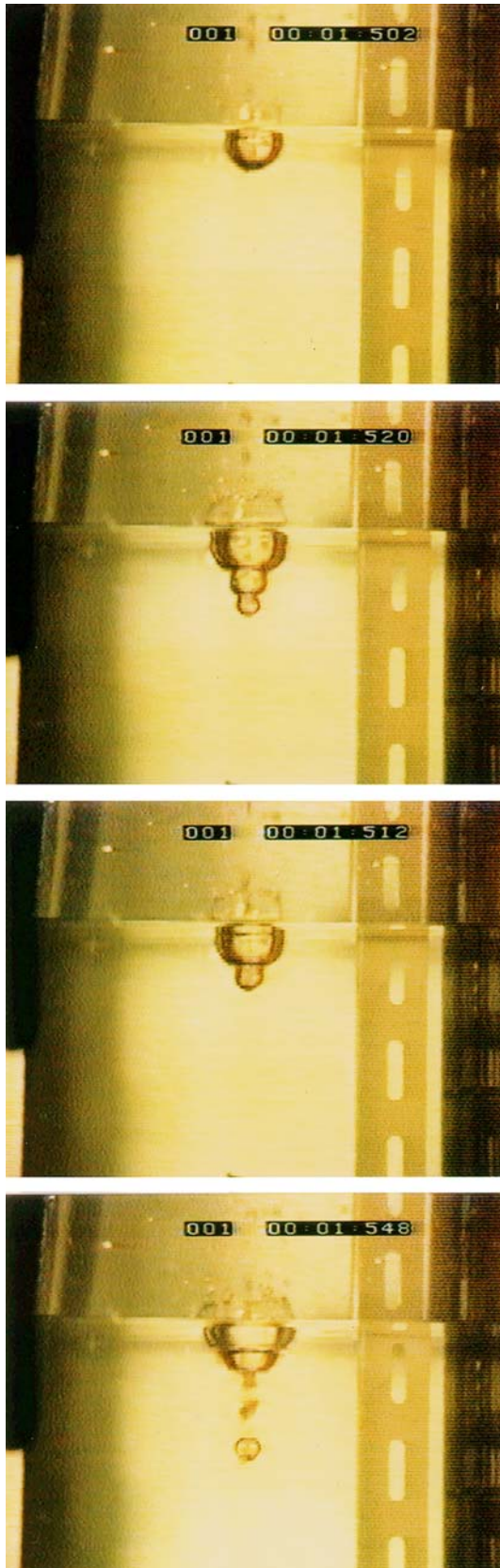
Fig. 2 A sequence of high-speed photographs of water droplets striking a free surface. The first droplet created a semi-spherical void at 502 ms. Two subsequent droplets each created a void at 512 and 520 ms. When the fourth droplet arrived at 548 ms, an air bubble separated from the void and was carried downward by the momentum of the droplet

impacting onto a pool of water is very different to that of droplet impact.

Figure 3 shows the time sequence of a water jet striking a free surface for test 6 (see Table 1); the filming speed was 2,000 frames per second. The water from the jet was dyed blue and thus appeared red in the negative images. The velocity of the impinging jet was 1.22 m/s.

The penetrating jet entrained air below the free surface and formed a conical air void surrounding the jet. The void grew in size and continued to deform in shape as the water jet penetrated the water. The water from the jet (appears red in negative image) was also found around the wall of the void. It is evident that during the period of jet penetration, the dyed water from the jet did not mix with the pool of water; instead, the water from the jet formed a layer around the void and separated the void from the surrounding water. Here movement of the lowest point of the interface is defined as the jet front and its velocity relative to the calm free surface is denoted as v_2.

A close-up view of the flow in the void created by an impinging water jet is presented in Fig. 4. After 99 ms the void stopped growing, and the dyed water from the jet began to break through the bottom of the void and enter the water below. At 140 ms, a tiny bubble pinched off from the void, leading the moving dye streak. As the dye streak moved downward, the void retracted towards the free surface. Turbulent mixing fully developed after 160 ms. A similar phenomenon was reported by Zhu et al. (1998, 2000) in a computer and experimental study of air entrainment induced by the perturbation of an otherwise steady column of water pouring into a free surface. It must be noted that before Zhu began his experiment a steady state in which a column of jet flowing into the free surface was established (that is, the free surface is calm). He then introduced a perturbation on the jet column. As the perturbed section of the jet entered the calm free surface an air void was created. Note that the jet front was absent in Zhu's case. However, we expect the shape of the void in Zhu's case to be similar to the void shown in Fig. 3 since both were created by the impact of bulbous sections of the jets.

When analysing the movement of the tip of the jet, an example of which is shown in Fig. 5, it was found that the tip had a velocity of v_j (jet velocity) as it entered the water, and was reduced to a constant velocity v_2 after impacting the free surface. This velocity, v_2, which was the velocity of the jet front, appeared to remain constant over the time interval where the void was expanding. The velocity ratio for the case shown in Fig. 3 is 0.627; velocity ratios measured for various tests in deep water

the point in time where the void, created by each droplet, achieved its maximum size. The next experiment will show that the mode of flow of a continuous jet

Fig. 3 A sequence of high-speed photographs for test 6 (see Table 1). The void created by air entrainment grew to a maximum size 99 ms after the impact. The jet then broke through the bottom of the void and carried a pinched off bubble downward (at 140 ms) while the void retracted to the free surface. Note that mixing of the two liquids occurred with the formation of turbulence after the void collapsed at about 160 ms after the impact. The velocity of the impinging jet was 1.22 m/s
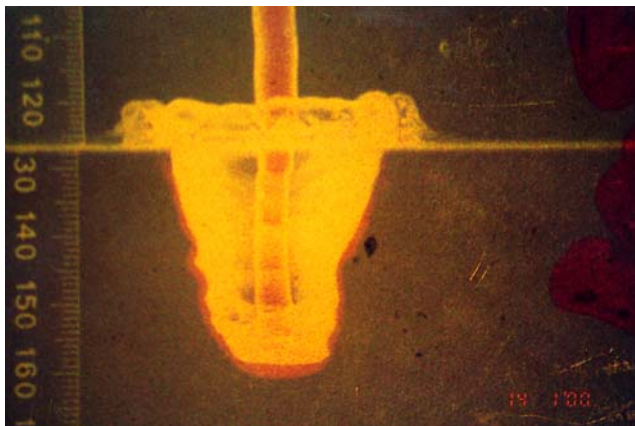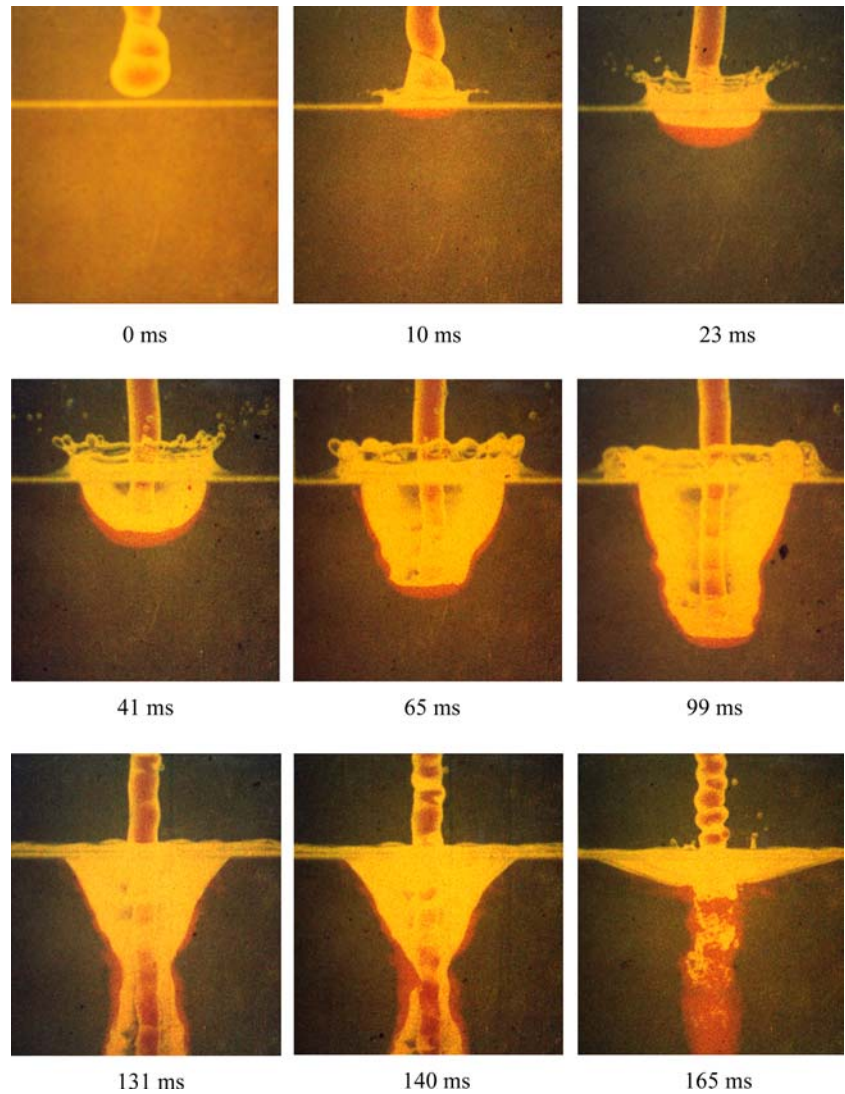

0 ms　　　　10 ms　　　　23 ms

41 ms　　　　65 ms　　　　99 ms

131 ms　　　　140 ms　　　　165 ms

Fig. 4 A close-up view of the results from test 6 at 99 ms after the impact. Water from the jet (*red*) formed a thin layer covering the inside of the void without mixing with the surrounding water
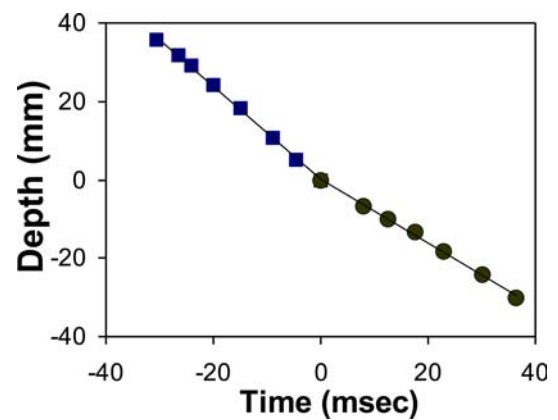

Fig. 5 Jet front distance from the calm free surface for test 6. Negative distance is above the free surface

experiments are tabulated in Table 1. Figure 6 shows the relationship between the velocity ratios and the Froude number (based on the diameter of the jet d_j) defined as:
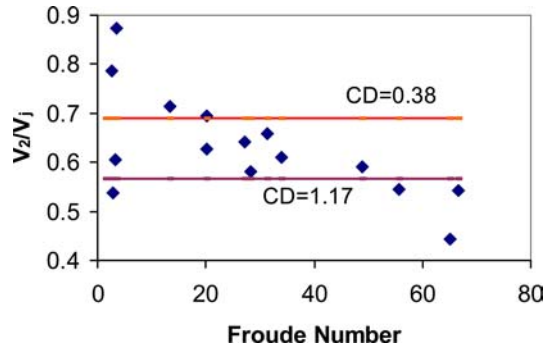$Fr = v_j^2 / (g d_j)$.

Fig. 6 Velocity ratio versus Froude number for a jet impinging at deep water. Results from the momentum analysis for a disc-like front (CD = 1.17) and a spherical front (CD = 0.38) are included for comparison

4 The analysis

The mathematical model for droplet impact so elegantly constructed by Pumphrey and Elmon (1990) is based on the conservation of energy at two instances when the fluid is assumed to be instantaneously at rest, namely, before the droplet begins to fall and when the void has reached it maximum volume. This is in contrast to the case of jet impact. As the jet continues to flow into the pool of water, it is not possible to construct an analysis similar to that of Pumphrey and Elmon (1990).

In the experiment conducted by Zhu et al. (1998, 2000), a steady stream of water column flowing into the free surface was established before the water column was perturbed to create a void on the free surface. As there was no moving front that can be identified, the analysis by Zhu took a different approach to the analysis presented here.

4.1 The conservation of momentum

The momentum equation may be applied with the following assumptions derived from observations in the experiments.

- The acceleration of the water jet due to gravity is negligible.
- The velocity of the water jet below the free surface remains constant with time.
- A quasi-steady state is assumed in the frame of reference which is moving with the velocity of the submerged jet.
- There is no mixing between the water in the jet and the water below the free surface.

The control volume in which the momentum equation applies consists of the section of the jet below the free surface. This is shown in the schematic diagram of Fig. 7. If the frame of reference is moving with the front of the jet, the flow around the surfaces of the jet and the void will appear to be steady free streamline flow. Thus, the velocity of water on the free surface around the jet
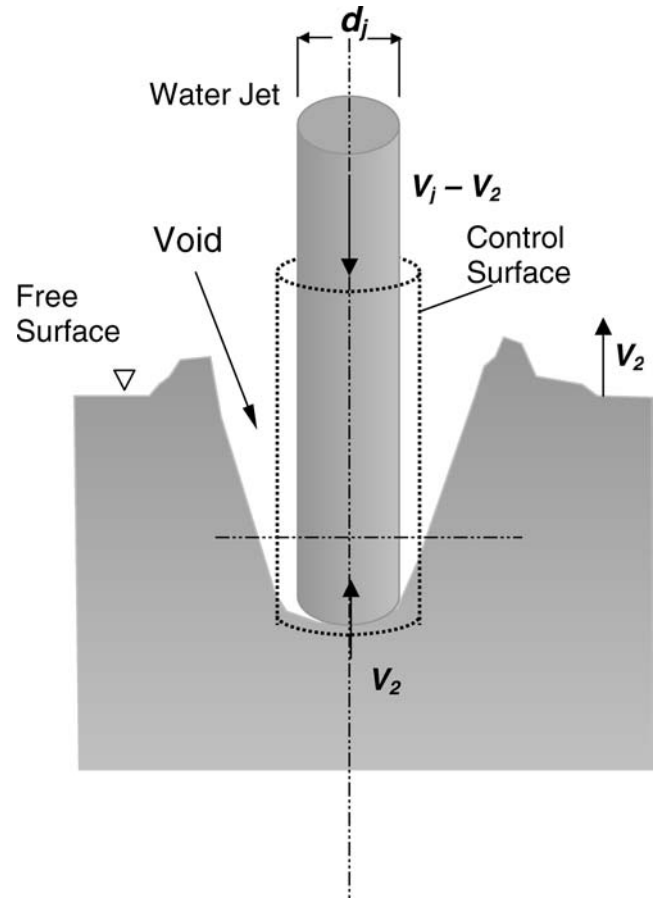

Fig. 7 Control volume for the momentum analysis of a water jet

front equals the relative velocity of the jet, that is, (v_j–v_2). The components that make up the momentum equation are the momentum flux $\rho A_j(v_j$–$v_2)^2$, the force due to pressure $\int_{A_j} p_2 dA$, and the body force $\rho A_j hg$. Here, p_2 is the pressure distribution around a streamline separating the water of the jet from the pool of water, ρ is the density of water, A_j is the cross-sectional area of the jet and h is its depth of penetration below the free surface. Hence the momentum equation takes the form:

$$\rho A_j \left(v_j - v_2 \right)^2 = \iint\limits_{A_j} p_2 dA - \rho A_j gh \tag{1}$$

where the integral on the right hand side of Eq. 1 represents the force due to pressure on the immersed jet front.

In this frame of reference, the free surface will appear to be moving with velocity v_2. The shape of the jet front will depend on the resistance between the two liquids as well as the pressure distribution on the front. From Bernoulli's equation, the pressure on the jet front, p_2, can be expressed in terms of the velocity, v, which is tangential to the interface:

$$p_2 = \rho gh + \tfrac{1}{2}\rho \left(v_2^2 - v_j^2 \right) \tag{2}$$

By substituting the expression for p_2 from Eq. 2, the integral on the right hand side of Eq. 1, can be integrated over the jet cross-section. The first term on the right in Eq. 2 yields the weight of the jet column and the second term can be expressed in terms of the drag coefficient, C_D, of the jet front:

$$\iint\limits_{A_j} p_2 dA = \rho A_j gh + \frac{1}{2}\rho A_j C_D v_2^2 \qquad (3)$$

The above equation consists of a buoyancy (statics) term and a form drag (dynamics) term. Note that the drag coefficient, C_D, is defined in a similar manner as that for a bluff body in super-cavitation flow.

Hence Eq. 1 becomes:

$$\left(1 - \frac{v_2}{v_j}\right)^2 = \frac{C_D}{2}\left(\frac{v_2}{v_j}\right)^2 \qquad (4)$$

It is worth noting that the value of C_D depends on the shape of the jet front which in turn depends on many factors including gravity, the jet speed and the initial shape of the jet before impact.

The theoretical value for the velocity ratio, v_2/v_j, also denoted by λ, is given by:

$$\lambda = \frac{v_2}{v_j} = \frac{1}{1 + \sqrt{C_D/2}} \qquad (5)$$

The values of the drag coefficient, C_D, may be estimated from known data. From the experiments, the measured jet diameters ranged from 5.7 to 7.5 mm and the velocities of the jet front vary from 0.16 to 1.2 m/s, which give Reynolds numbers in the range of 300–7,000. The shape of the jet front can be considered to take a form between a smooth sphere and a flat circular disc. At Reynolds number above 1,000, where the contribution of viscous force is insignificant compared with that of pressure, the drag coefficient of a disc normal to the flow is 1.17 and for a smooth sphere it is 0.38 (Hoerner 1965). Substitution of these values into Eq. 5 yields the velocity ratios of 0.567 and 0.691, respectively. These are also shown in Fig. 6. With the exception of very low Froude number ($Fr < 3$), where surface tension may be important, it is evident that the experimental results fall close to the range of these two values. Note that one unusual result came from the point for Froude number 65.1 where the velocity ratio is 0.443. This is due to the impinging jet which stopped flowing into the water before the void reached its maximum volume.

The tendency for surface tension is to produce a rounded head of the jet, whereby the rounding process introduces unsteady motions on the bulbous head of the jet, and upon impact causes variations in the initial shape of the void. It follows that the mode of propagation of a free surface wave varied according to the initial shape of the void. This led to some scattering of the data. It should be noted that it was difficult to control the shape of the jet front during the free fall of the jet.

4.2 The conservation of energy

In their study of the hemispherical air void below a free surface created by a falling water droplet, Pumphrey and Elmon (1990) assumed that the kinetic energy of the surrounding fluid was zero when the air void created by the impact of the water droplet was at its maximum volume. In this way, the potential energy of the droplet can be related to the instant when the flow has reached static equilibrium—that is, when the size of the hemispherical void created by the droplet is at its maximum. The analysis using energy conservation applied in the case of jet impingement on a free surface will take a different approach. The control volume will be the fluids (water and air) below the calm free surface. Hence, the control surface is a horizontal plane which coincides with the calm free surface.

The unsteady energy equation with no heat transfer, in the convention as defined by Fox and MacDonald (1998), is given by:

$$\dot{W} + \frac{\partial}{\partial t}\iiint\limits_{\substack{\text{control}\\\text{volume}}} \rho e\, d\forall + \iint\limits_{\substack{\text{control}\\\text{surface}}} \rho e \vec{v}\, d\vec{A} = 0 \qquad (6)$$

The first term on the left, $\dot{W}$ is the work done by the atmospheric pressure in deforming the free surface and is expressed as a surface integration in Eq. 7 which consists of the atmospheric pressure, p_{atm}, the velocity vector $\vec{v}$ and the area vector, $\vec{A}$. Since the atmospheric pressure is uniform and there is no net change of volume of water inside the control surface:

$$\dot{W} = \iint\limits_{\substack{\text{control}\\\text{surface}}} p_{atm}\vec{v}\, d\vec{A} = 0 \qquad (7)$$

The second term on the left in Eq. 6 involves the specific energy, e, in the control volume. For incompressible flow, it is given by:

$$e = \frac{v^2}{2} + gz \qquad (8)$$

where z is the vertical height measured upward from the free surface; thus, the value of z for a point in the control volume is negative.

Hence the integration over the control volume for the second term yields the expression:

$$\frac{\partial}{\partial t}\iiint\limits_{\substack{\text{control}\\\text{volume}}} \rho e\, d\forall = \frac{\partial}{\partial t}\iiint\limits_{\substack{\text{control}\\\text{volume}}} \rho\left[\frac{v^2}{2}\right] d\forall + \frac{\partial}{\partial t}\iiint\limits_{\substack{\text{control}\\\text{volume}}} \rho[gz] d\forall$$

$$= \frac{\partial}{\partial t}\left[\rho\frac{v_j^2}{2}A_j h(t)\right] + \dot{K}(t) + \rho g\frac{\partial}{\partial t}[M] \qquad (9)$$

where M is the moment of the volume of the void and the moment is taken about the free surface.

Note that the integration of the term involving ρv^2 gives rise to two components: the kinetic energy of the jet with cross-section area A_j in the air void of height $h(t)$, and the kinetic energy $K(t)$ of the water in the control volume excluding that of the water jet. The integration of the term involving ρgz yields the first moment of the weight of the control volume, ρgM, about the free surface. Since z is negative below the free surface, M is a negative quantity.

The third term of Eq. 6 is dominated by the kinetic energy flux of the jet. The fluxes of the kinetic energy and the potential energy across the control surface are assumed negligible; thus,

$$\iint\limits_{\substack{\text{control}\\\text{surface}}} \rho e \vec{v} \mathrm{d}\vec{A} = \iint\limits_{\substack{\text{control}\\\text{surface}}} \rho \left[\frac{v^2}{2} + gz\right] \vec{v} \mathrm{d}\vec{A} = -\rho A_j \frac{v_j^2}{2} v_j$$

(10)

The result of the integration is negative since the jet is entering the free surface from above.

The terms in Eq. 6 are replaced by Eqs. 7, 9 and 10, respectively, giving

$$\frac{\partial}{\partial t}\left[\rho \frac{v_j^2}{2} A_j h(t)\right] + \dot{K}(t) + \rho g \frac{\partial}{\partial t}[M] - \rho A_j \frac{v_j^2}{2} v_j = 0 \quad (11)$$

The above equation can be integrated with respect to time. Observation revealed that the depth of the void grew with a constant velocity, v_2, hence the time variable, t, can be replaced by $h(t)/v_2$, giving

$$\left[\rho \frac{v_j^2}{2} A_j h(t) + K(t) + \rho g|M(t)|\right] - \rho A_j \frac{v_j^2}{2} v_j \frac{h(t)}{v_2} = 0 \quad (12)$$

Since $|M(t)|$ is the moment of the volume of the void, the term $\rho g|M(t)|$ represents the moment of the weight of water displaced by the void.

The above is re-arranged and the ratio, v_2/v_j, is replaced with λ:

$$\frac{Fr}{2}\left[\frac{1}{\lambda} - 1\right] - \frac{|M(t)|}{A_j h(t) d_j} = \frac{K(t)}{\rho g A_j d_j h(t)} \quad (13)$$

Note that $K(t)$, which is the kinetic energy in the water surrounding the void, and $|M(t)|$, the moment of volume of the void, are both positive quantities. If the void is prismatic in shape, then $|M(t)|$ is proportional to $[h(t)]^2$ On the other hand $|M(t)|$ is proportional to $[h(t)]^4$ if the dimensions of the void are proportional to its height. At any rate, the magnitude of the second term on the left hand side of Eq. 13 will increase with $h(t)$. Experiments showed that the velocity ratio λ remained constant throughout the growth period of the void; hence, the first term on the left hand side of Eq. 13 is a

constant independent of time. It follows that the moment of the void, $|M(t)|$ will continue to increase with the result that the value of $K(t)$ will continue to diminish. However, the conservation of energy will demand that the kinetic energy, $K(t)$, is positive definite; hence, the void can only grow to a maximum size and beyond this point it will contract as the jet breaks through the void to enter the water below, as observed in the experiments.

The maximum limit for the height of a void, $h(t)$, can be estimated from Eq. 13 by setting $K(t)$ to zero. For a void which occupies a volume enclosed by a conical shape and a water jet which is cylindrical in shape with diameter d_j, its moment $|M(t)|$ is given by:

$$|M(t)| = G[h(t)]^4 - \frac{A_j}{2}[h(t)]^2 \quad (14)$$

where $G[h(t)]^4$ is the moment of the conical volume about its base.

The maximum height, h_m, satisfies the following equation:

$$\frac{Fr}{2}\left[\frac{1}{\lambda} - 1\right] - \frac{4Gh_m^3}{\pi d_j^3} + \frac{h_m}{2d_j} = 0 \quad (15)$$

Equation 15 is cubic in h_m/d_j and its root can be obtained from the Cardan's method of solution which gives:

$$\frac{h_m}{d_j} = \left[\frac{\pi Fr}{8G}\left(\frac{1-\lambda}{\lambda}\right)\right]^{1/3}$$
$$\times \left\{\left[1 + \sqrt{1 - \frac{\pi}{54GFr^2}\left(\frac{\lambda}{1-\lambda}\right)^2}\right]^{1/3}\right.$$
$$\left. + \left[1 - \sqrt{1 - \frac{\pi}{54GFr^2}\left(\frac{\lambda}{1-\lambda}\right)^2}\right]^{1/3}\right\} \quad (16)$$

An illustration on the use of Eq. 16 is presented in the Appendix. The value of G is estimated from the images and, together with Fr and λ, produce the estimated value of h_m/d_j. These values are compared with the results from direct measurement. As expected from the assumption of zero kinetic energy (setting $K(t)$ to zero) mentioned earlier, Eq. 16 over predicts the maximum height to jet diameter ratio with an exception of one case where the Froude number is the lowest.

For large Froude number, that is $\frac{54GFr^2}{\pi}\left(\frac{1-\lambda}{\lambda}\right)^2 > 1$, the above value of h_m/d_j is approximately:

$$\frac{h_m}{d_j} \approx \left[\frac{\pi}{8G}\left(\frac{1-\lambda}{\lambda}\right)\right]^{1/3}\left\{Fr^{1/3} + \left[\frac{\pi}{54G}\left(\frac{\lambda}{1-\lambda}\right)^2\right]^{1/3}Fr^{-1/3}\right\} \quad (17)$$

and for a small value of Fr, it is:

$$\frac{h_{\mathrm{m}}}{d_{\mathrm{j}}} \approx 2\left[\frac{\pi}{8G}\left(\frac{1-\lambda}{\lambda}\right)\right]^{1/3} Fr^{1/3} \qquad (18)$$

However, it must be noted that surface tension effects may not be negligible in the case where the Froude number is small.

Zhu et al. (2000) gave the expression for $h_{\mathrm{m}}/d_{\mathrm{j}}$ in the form:

$$\frac{h_{\mathrm{m}}}{d_{\mathrm{j}}} \approx \frac{1}{4}\left(\frac{D_{\mathrm{c}}}{d_{\mathrm{j}}}\right)^{2/3} Fr^{1/3} + 1.8(Fr)^{1/4} \qquad (19)$$

where D_{c} is the diameter of the base of the void.

It can be said that the first term varies with the 1/3-power of Fr in the same way as the results given in Eqs. 16, 17 and 18.

5 Concluding remarks

The visualization study showed that a void is formed as a water jet impacts a pool of water. Of interest are the shapes of the entrained void. The effects of surface tension mold the tip of the jet into a globular form. As a result, the initial impact is similar to that between a droplet and a free surface; hence the void is initially hemispherical in shape. Further addition of jet momentum elongates the void into a conical form. The void grows to a maximum volume and subsequent instability causes it to collapse and the mixing of the two fluids will then occur. There was no evidence of mixing between the water in the impinging jet and the bulk of water during the formation of the void. It is also found that during the growing phase of the void, the velocities of the jet fronts remain constant and are not affected by gravity.

The above observations allow application of the conservation of momentum to produce Eq. 5, which shows that the velocity ratio is only dependent on the drag coefficient of the jet front. The absence of the height of the air void, $h(t)$, in the equation further confirms the observations that the velocity ratio should remain constant during the growing phase of the void. Note also that the shape of the jet as it impacts onto the water is represented by its corresponding drag coefficient in Eq. 5. Figure 6 demonstrated that the predicted values of v_2/v_{j} agreed with the experimental results for a possible variation of the shape of the jet front.

The study by Zhu et al. (2000) on air entrainment caused by perturbing an otherwise laminar jet has indicated that the energy for creating the void is larger than that in the perturbed section of the jet. It is concluded that, after the perturbed jet created the void, the following laminar jet will continue to feed energy into the void to sustain its growth. In the same way, the air voids shown in Figs. 2 and 4 were created by the impact of the globular fronts of the impinging jets and were sustained for a finite time by the energy of the water jets. The conservation of energy gives rise to Eq. 13, which shows that the maximum height of the void is predominantly proportional to one-third power of the Froude number.

The effects of surface tension may be accounted for by including, on the left hand side of Eq. 13, a term which consists of the product of the surface tension and the surface area of the void.

6 Appendix

The images of the experiments may be analyzed further to yield data that enable G to be calculated. Instead of calculating the first moment of the void at the time of breaking up by measuring its exact shape, we assume that the shape of the void is close to that of a truncated cone. The base diameter of the cone, D_{c}, is the diameter of the void at the free surface. The smaller circular surface of the truncated cone with have a diameter equal to the diameter of the jet, d_{j}. The height of the cone is h_{m}. The first moment of the truncated cone about its base diameter is given by:

$$G = \frac{\pi}{48}\left(\frac{D_{\mathrm{c}}}{h_{\mathrm{m}}}\right)^2 \left\{ \left(\frac{D_{\mathrm{c}}}{D_{\mathrm{c}}-d_{\mathrm{j}}}\right)^2 \right.$$
$$\left. - \left(\frac{d_{\mathrm{j}}}{D_{\mathrm{c}}}\right)^2\left[\frac{4d_{\mathrm{j}}}{D_{\mathrm{c}}-d_{\mathrm{j}}} + \left(\frac{d_{\mathrm{j}}}{D_{\mathrm{c}}-d_{\mathrm{j}}}\right)^2\right]\right\} \qquad (20)$$

Table 2 Jet impingement into deep water—continuation from Table 1

Test no.	Fr	λ	h_{m}	D_{m}	d_{j}	$h_{\mathrm{m}}/d_{\mathrm{j}}$	$h_{\mathrm{m}}/d_{\mathrm{j}}$(calc)
1	2.6	0.787	14.5	15.5	5.8	2.500	2.309
2	2.8	0.538	9.5	12.9	5.7	1.667	2.218
3	3.3	0.605	13.8	16.4	5.6	2.462	2.596
4	3.5	0.872	10.3	12.3	5.9	1.750	1.847
5	13.3	0.714	17.6	14.4	5.9	3.000	4.043
6	20.1	0.627	20.0	29.0	7.5	2.667	3.667
7	20.2	0.695	21.4	21.4	6.5	3.292	4.274
8	27.2	0.642	24.0	31.5	7.5	3.200	4.281
9	28.4	0.581	21.8	17.0	6.5	3.354	6.099
10	31.3	0.659	27.5	32.5	7.5	3.667	4.726
11	34.1	0.611	28.3	23.1	6.5	4.354	6.452
12	48.9	0.591	29.5	35.0	7.5	3.933	5.940
13	55.7	0.544	46.5	24.9	6.5	7.154	11.040
14	65.1	0.443	33.3	26.6	6.5	5.123	10.044
15	66.6	0.543	40.4	25.9	6.5	6.215	10.348

Fr Froude number; λ velocity ratio; h_{m} maximum depth of void; D_{m} void diameter on free surface; d_{j} jet diameter; $h_{\mathrm{m}}/d_{\mathrm{j}}$(calc) value of the ratio calculated from Eq. 16.

Thus G can be calculated from the values of h_m, D_c and d_j, which are measured at the moment the void reaches it maximum height. The value of G is substituted into Eq. 16 to yield the upper limit of the ratio h_m/d_j.

Table 2 is the continuation of Table 1; it contains the measured values of h_m, D_c and d_j. The ratio h_m/d_j is compared with h_m/d_j(calc), which is calculated from Eq. 16. It is evident that, h_m/d_j(calc) over-predicted the value of h_m/d_j; however, the exception is test 1 where the Fr is the lowest.

Table 2 shows the extent the theory deviated from the measurements. The calculated values appear to be in good agreement with measurements for $Fr < 10$, are about 30% too high for Fr around 20, and are over 50% too high for $Fr > 50$.

References

Benjamin TB, Ellis AT (1966) The collapse of cavitation bubbles and the pressure thereby produced against solid boundaries. Philos Trans R Soc Lond A 260:221–240

Best JP (1993) The formation of toroidal bubbles upon the collapse of transient cavities. J Fluid Mech 251:79–107

Bonetto F, Drew D, Lahey RT Jr (1994) The analysis of a plunging liquid jet—the air entrainment process. Chem Eng Commun 130:11–29

Cummings PD, Chanson H (1997) Air entrainment in the developing flow region of plunging jets—part 1: theoretical development. J Fluid Eng 119:597–602

Fox RW, McDonald AT (1998) Introduction to fluid mechanics, 5th edn. Wiley, New York, pp 155–157

Hoerner SF (1965) Fluid dynamic drag, 2nd edn. Midland Park, NJ

Oguz HN, Prosperetti A, Kolaini AR (1995) Air entrapment by a falling water mass. J Fluid Mech 294:181–207

Pumphrey HC, Elmon PA (1990) The entrainment of bubbles by drops impacts. J Fluid Mech 220:539–567

Zhang S, Duncan JH, Chaline GL (1993) The final stage of the collapse of a cavitation bubble near a rigid wall. J Fluid Mech 257:147–181

Zhu Y, Oguz HN, Prosperetti A (1998) Mechanism of air entrainment by an impinging liquid jet. In: Thompson MC, Hourigan K (eds) Thirteenth Australasian fluid mechanics conference, Monash University, Australia, December, pp 337–340

Zhu Y, Oguz HN, Prosperetti A (2000) On the mechanism of air entrainment by liquid jets at a free surface. J Fluid Mech 404:151–177